




Mutagenesis Mapping of RNA Structures within the Foot-and-Mouth Disease Virus Genome Reveals Functional Elements Localized in the Polymerase (3D^{pol})-Encoding Region

 Lidia Lasecka-Dykes,^a Fiona Tulloch,^{b*}  Peter Simmonds,^c Garry A. Luke,^b Paolo Ribeca,^{a*} Sarah Gold,^a Nick J. Knowles,^a Caroline F. Wright,^a Jemma Wadsworth,^a Mehreen Azhar,^a Donald P. King,^a Tobias J. Tuthill,^a Terry Jackson,^a Martin D. Ryan^b

^aThe Pirbright Institute, Pirbright, Surrey, United Kingdom

^bBiomedical Sciences Research Complex (BSRC), School of Biology, University of St. Andrews, St. Andrews, United Kingdom

^cNuffield Department of Experimental Medicine, University of Oxford, Oxford, United Kingdom

Lidia Lasecka-Dykes and Fiona Tulloch contributed equally to this work. Author order was agreed upon by all authors.

ABSTRACT RNA structures can form functional elements that play crucial roles in the replication of positive-sense RNA viruses. While RNA structures in the untranslated regions (UTRs) of several picornaviruses have been functionally characterized, the roles of putative RNA structures predicted for protein coding sequences (or open reading frames [ORFs]) remain largely undefined. Here, we have undertaken a bioinformatic analysis of the foot-and-mouth disease virus (FMDV) genome to predict 53 conserved RNA structures within the ORF. Forty-six of these structures were located in the regions encoding the nonstructural proteins (nsps). To investigate whether structures located in the regions encoding the nsps are required for FMDV replication, we used a mutagenesis method, CDLR mapping, where sequential coding segments were shuffled to minimize RNA secondary structures while preserving protein coding, native dinucleotide frequencies, and codon usage. To examine the impact of these changes on replicative fitness, mutated sequences were inserted into an FMDV subgenomic replicon. We found that three of the RNA structures, all at the 3' termini of the FMDV ORF, were critical for replicon replication. In contrast, disruption of the other 43 conserved RNA structures that lie within the regions encoding the nsps had no effect on replicon replication, suggesting that these structures are not required for initiating translation or replication of viral RNA. Conserved RNA structures that are not essential for virus replication could provide ideal targets for the rational attenuation of a wide range of FMDV strains.

IMPORTANCE Some RNA structures formed by the genomes of RNA viruses are critical for viral replication. Our study shows that of 46 conserved RNA structures located within the regions of the foot-and-mouth disease virus (FMDV) genome that encode the nonstructural proteins, only three are essential for replication of an FMDV subgenomic replicon. Replicon replication is dependent on RNA translation and synthesis; thus, our results suggest that the three RNA structures are critical for either initiation of viral RNA translation and/or viral RNA synthesis. Although further studies are required to identify whether the remaining 43 RNA structures have other roles in virus replication, they may provide targets for the rational large-scale attenuation of a wide range of FMDV strains. FMDV causes a highly contagious disease, posing a constant threat to global livestock industries. Such weakened FMDV strains could be investigated as live-attenuated vaccines or could enhance biosecurity of conventional inactivated vaccine production.


KEYWORDS CDLR-based mutagenesis, RNA structure, bioinformatics, foot-and-mouth disease virus (FMDV), viral replication

Citation Lasecka-Dykes L, Tulloch F, Simmonds P, Luke GA, Ribeca P, Gold S, Knowles NJ, Wright CF, Wadsworth J, Azhar M, King DP, Tuthill TJ, Jackson T, Ryan MD. 2021. Mutagenesis mapping of RNA structures within the foot-and-mouth disease virus genome reveals functional elements localized in the polymerase (3D^{pol})-encoding region. *mSphere* 6:e00015-21. <https://doi.org/10.1128/mSphere.00015-21>.

Editor Urs F. Greber, University of Zurich
© Crown copyright 2021. This is an open-access article distributed under the terms of the [Creative Commons Attribution 4.0 International license](https://creativecommons.org/licenses/by/4.0/).

Address correspondence to Lidia Lasecka-Dykes, lidia.dykes@pirbright.ac.uk, or Martin D. Ryan, mdr1@st-andrews.ac.uk.

* Present address: Fiona Tulloch, Benchmark Animal Health, Edinburgh, Scotland, United Kingdom; Paolo Ribeca, Biomathematics and Statistics Scotland, Edinburgh, Scotland, United Kingdom.

 Identification of novel RNA structures essential for replication of foot-and-mouth disease virus (FMDV) @Lidia_Lasecka

Received 13 January 2021

Accepted 16 June 2021

Published 14 July 2021

The genomes of RNA viruses not only encode proteins but also contain nontemplated functional elements in both the coding and untranslated regions (UTRs). These elements can be secondary or higher-order RNA structures such as simple stem-loops or more complex structures which include pseudoknots and so-called kissing loops that mediate long-range RNA-RNA interactions (1–12). The function, shape, and number of such RNA functional elements are often characteristic for a particular group of viruses, where they play important roles in processes such as the initiation of viral RNA translation and replication, subgenomic mRNA transcription, frameshift events, viral RNA encapsidation, and modulation of host's antiviral responses (reviewed in reference 13). Since many RNA viruses are of medical and veterinary importance, characterization of these RNA structures brings us closer to understanding viral pathogenicity and provides opportunities for disease control.

Foot-and-mouth disease virus (FMDV) is the causative agent of foot-and-mouth disease (FMD), a highly contagious disease of cloven-hoofed animals (including livestock) (reviewed in reference 14). FMD is endemic in Africa and Asia, where it impacts upon productivity and trade as well as posing a constant threat of causing costly incursions into disease-free countries (15–21). Control of FMD by vaccination in endemic settings is complicated by the high antigenic variability of the seven serotypes of FMDV: A, Asia 1, C (not reported since 2004), O, Southern African Territories 1 (SAT 1), SAT 2, and SAT 3 (19, 20, 22–24).

FMDV is a small nonenveloped positive-sense single-stranded RNA virus classified in the species *Foot-and-mouth disease virus*, genus *Aphthovirus* in the family *Picornaviridae*. The FMDV genome is ~8.5 kb in size and composed of a single, long open reading frame (ORF) which is flanked by 5' and 3' UTRs (reviewed in reference 25). The encoded polyprotein is co- and posttranslationally cleaved by viral proteases (L^{pro} and $3C^{pro}$) and by a ribosomal skipping event mediated by the 2A peptide into a number of functional precursors and the mature proteins (26–34). The coding sequence for the FMDV ORF is arbitrarily divided into four regions (5'- L^{pro} , P1, P2, and P3-3'). The P1 region encodes the capsid proteins (1A, 1B, 1C, and 1D, also called VP4, VP2, VP3, and VP1, respectively), while the P2 and P3 regions encode the nonstructural proteins (nsps) (reviewed in reference 25).

There are several RNA structures within picornavirus genomes that have been bioinformatically predicted and characterized biochemically (12, 35–39). These structures are predominantly located in the UTRs and have been shown to be important for replication and translation of picornavirus genomes (reviewed in reference 40). Within the 5' UTR of the FMDV genome, the S-fragment forms a single, long hairpin structure (293 to 381 nucleotides [nt] in length) and has been reported to play a role in viral replication and innate immune modulation (41–45). Elsewhere in the 5' UTR, the presence of multiple (two to four) pseudoknots downstream of the poly(C) tract has been shown to determine virus tropism (41, 46). Other key and well-characterized RNA structural elements include a type II internal ribosome entry site (IRES), which initiates cap-independent translation of the viral genome (41, 47–50), while the *cis*-acting replication element (*cre*) acts as a template for uridylylation of the VPg (3B) protein, which then acts as a primer for synthesis of viral RNA (51, 52). The 3' UTR of the FMDV genome is located upstream of the poly(A) tract and contains two RNA stem-loop structures called SL1 and SL2. These stem-loops interact nonsimultaneously with the S-fragment and IRES, forming long-range interactions that have been shown to be necessary for viral RNA replication (43, 53, 54).

A number of other secondary RNA structures have been predicted computationally to be present within the FMDV ORF (12). However, with the exception of packaging signals (55), the role(s) of these structures in the FMDV replication cycle has not been determined. In this study, we have identified 46 evolutionarily conserved RNA structures within the regions of the FMDV ORF that encode the nsps. Mutagenesis of these structures identified three novel RNA stem-loops in the coding region of the RNA-dependent RNA polymerase ($3D^{pol}$) that are essential for replication of an FMDV

subgenomic replicon, suggesting that these structures are required for either initiation of viral RNA translation and/or viral RNA synthesis. In contrast, mutagenesis of the remaining 43 structures had no effect on replicon replication. This approach can aid in the identification of critical viral RNA structures required for viral genome replication and also help identify conserved RNA structures that are not essential for virus replication that could provide ideal targets for the rational attenuation of a wide range of FMDV strains.

RESULTS

Prediction of conserved RNA structures within the FMDV genome. While previous studies have provided evidence that the FMDV genome is highly structured with conserved RNA base pairing throughout the coding part of the genome (12, 56), these studies were conducted on a relatively small data set. Since the number of full genome sequences available on public databases has greatly increased in recent years, before conducting functional studies, we revisited these analyses to predict conserved RNA stem-loops that were common in 118 representative genomic sequences covering all FMDV serotypes (see Table S1 in the supplemental material).

The degree of RNA structure formation in the FMDV genome was estimated bioinformatically through calculation of minimum free energies (MFEs) of the most thermodynamically stable *in vitro* folded RNA sequences (57–59). However, MFE values on their own do not suffice to demonstrate the existence of biologically relevant structures, because they are conditioned by compositional factors, such as G+C content and dinucleotide representation in addition to base order. To account for this, the mean folding energy difference (MFED) metric was developed (60–62), in which MFE values of native sequences are compared to those randomized in base order but preserving mono- and dinucleotide frequencies (the algorithm NDR in the current study [56]). High MFED values are indicative of regions with base order-dependent and potentially biologically relevant RNA secondary structure.

Using this approach, all 118 FMDV genomic sequences in their genomic (positive-sense) orientations were scanned using the program Fold Energy Scan in the SSE package (63) to calculate MFED values. This analysis employed an incremental sliding window computation with user-defined window size and increment (63) (in our case, 400 and 20 nt, respectively, where each 400-nt segment overlapped its neighbors by 380 nt). Despite the high genomic sequence diversity across all seven serotypes (20% mean nucleotide pairwise distance [\pm 9% standard deviation {SD}], with 31% [\pm 5% SD] and 14% [\pm 7% SD]) average pairwise distance in the regions encoding the capsid proteins and the nsps, respectively), all the FMDV genomes analyzed showed high folding energies across most of their sequence compared to the NDR-permuted controls (Fig. 1A). This indicates that all FMDV sequences possess similar extents of sequence order-dependent RNA secondary structure. To confirm this, full genome sequences were grouped into those of Eurasian (A, Asia 1, C, and O serotypes) and SAT (SAT 1 to 3 serotypes) origin, and average MFED values were determined along the genome for each group. Although we recognize that the grouping may not completely accommodate the interserotypic history of these viruses (genomes of several isolates of SAT serotypes contain 5' UTR and regions encoding nsps which are phylogenetically more closely related to corresponding genomic regions of Eurasian isolates than of other SAT isolates) (45), the MFED plots showed similar patterns of high and low MFED values across the genome. MFED values were better correlated between FMDV groups in the UTRs and the regions encoding the nsps, identifying a potentially greater degree of RNA structure conservation compared to the more genetically divergent region encoding the capsid proteins (Fig. 1B).

The window size used for MFED scanning does not identify individual RNA structures and only highlights regions with high folding energies (which may contain dissimilar structures and/or structures located at different positions). Therefore, RNAalifold program, implemented in the ViennaRNA Package (64), was used to identify

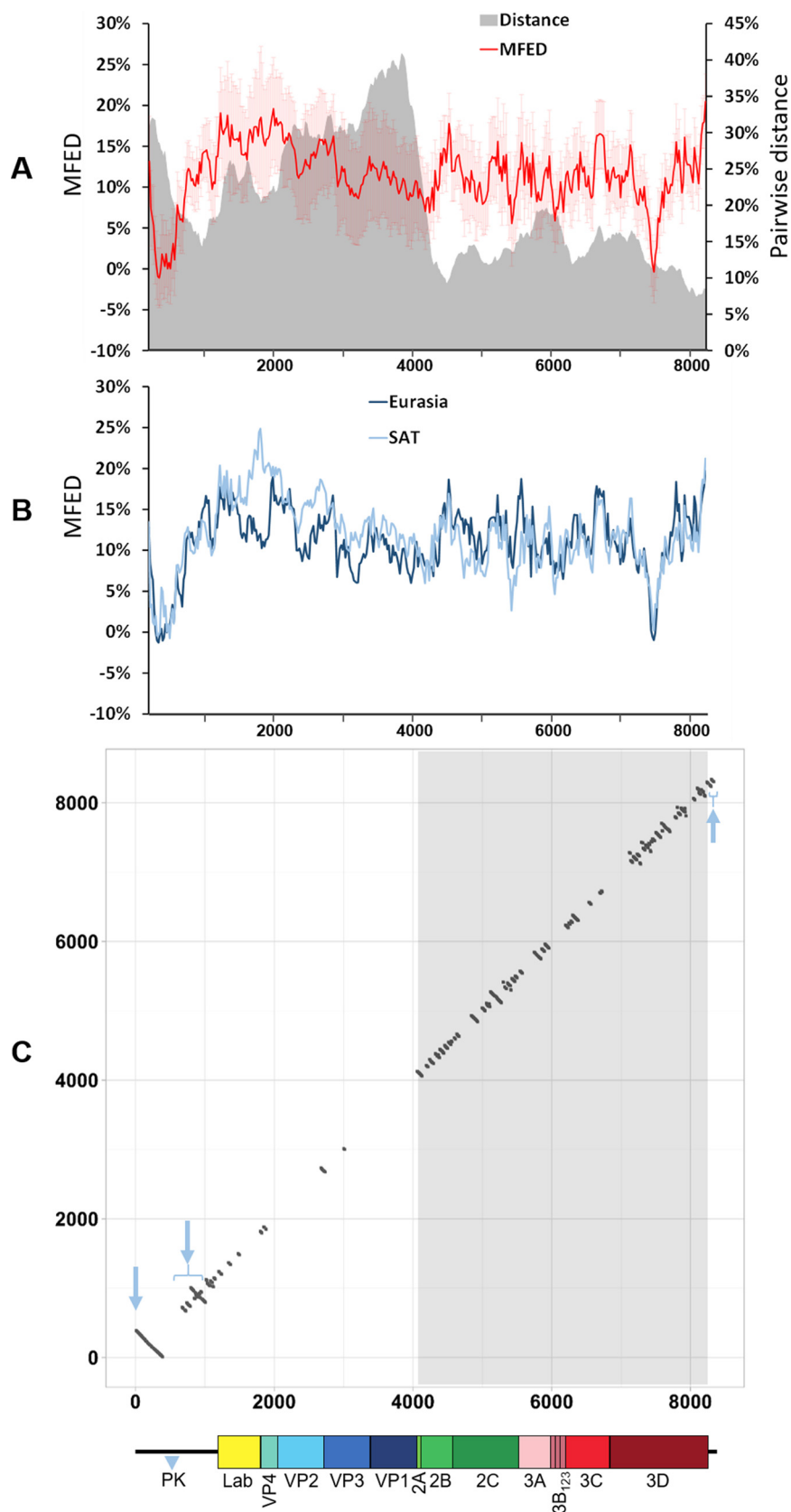


FIG 1 Extent of the conserved RNA secondary structures within the FMDV genome. (A) A scan of pairwise distance (in gray) and mean folding energy difference (MFED) (in red) prepared using SSE v1.4 software and 118 FMDV sequences representing all seven serotypes. The mean values for
(Continued on next page)

individual conserved RNA stem-loops for all 118 whole genomic sequences and, separately, also for the sequences grouped into each FMDV serotype individually. Stem-loops conserved for all seven serotypes were visualized as a dot plot graph, plotting each nucleotide pairing (represented by individual dots) against positions of involved nucleotides on the x and y axes (Fig. 1C). Any pairing interactions distanced by more than 400 nt were removed after analysis. By excluding long-distance interactions after whole-genome RNA structure prediction, we did not ignore the effect they may have on formation of local pairings. RNAalifold cannot predict pseudoknots, and therefore, the region directly downstream of the poly(C) tract was excluded from our analyses (Fig. 1). The presence of each conserved stem-loop was then further verified in each FMDV genomic sequence tested (Table S2).

These analyses correctly predicted the presence of well-characterized RNA secondary structures in the FMDV genome: the S-fragment, IRES, and *cre*, all located in the 5' UTR, and SL1 and SL2 located in the 3' UTR (Fig. 1C; see also Fig. S1 in the supplemental material). It additionally identified several serotype-specific conserved stem-loops in the region encoding the capsid proteins, but only four of these were conserved in all seven serotypes (Table S2). In contrast, 46 stem-loops (when counting each RNA hairpin individually, even within a single branched structure) were universally present within the regions encoding the nsps (Fig. 1C and Table S2). Overall, there were 53 highly conserved stem-loops in the ORF of the FMDV genome that were conserved across all seven serotypes, with average conservation in 95% of FMDV isolates tested ($\pm 7\%$ SD [Table S2]).

Use of CDLR mutagenesis for functional mapping of predicted RNA structures.

Next, we undertook mutagenesis studies to investigate whether any of the conserved RNA structures identified in the FMDV genome play a functional role in viral replication. FMDV replicons lack the region encoding the capsid proteins but are replication competent, demonstrating that there are no RNA elements essential for translation or replication of viral RNA within the capsid-encoding region. Therefore, our investigation focused on structures located within the regions encoding the nsps of the replicon. Additionally, the effect on replication of changes incorporated into the replicon can be analyzed in real time through monitoring of fluorescence from an integrated green fluorescent protein (GFP) reporter gene that replaced the region encoding the capsid proteins (65).

In order to mutate the conserved RNA structures predicted within the regions encoding the nsps while maintaining codon composition, codon order, and dinucleotide frequencies of the native wild-type (WT) replicon sequence, we applied the CDLR scrambling method (11, 56). To monitor its effectiveness in altering or otherwise disrupting RNA pairing within the native sequence, sequence of the regions encoding the nsps of WT replicon was randomly permuted 50 times using the CDLR algorithm. Then, MFED values for these mutants were calculated as described above, and these values were compared to MFED values of the native WT replicon sequence and the corresponding sequences of the 118 FMDV isolates used in this study. Sequences generated by CDLR showed evidence of severely disrupted RNA secondary structures, with a

FIG 1 Legend (Continued)

successive 400-nt fragments across the genome are plotted (where each 400-nt segment overlapped its neighbors by 380 nt). The light red shading represents error bars showing standard deviations from the mean for each MFED data point. The y axis shows genome nucleotide position. (B) MFED values for the same FMDV genomic sequences but grouped into Eurasian (A, Asia 1, C, and O serotypes) (dark blue) or SAT (SAT 1 to 3 serotypes) (light blue) clusters. (C) A dot plot graphical representation of RNA structures that were conserved across all seven FMDV serotypes. The x axis and y axis represent FMDV genome positions, with each dot representing a single pairing between two nucleotides, one with its position marked on the x axis and the other one with its position marked on the y axis. The three pale blue arrows indicate the locations of the S-fragment, *cre* plus IRES, and SL1 plus SL2 structures on the dot plot graph, respectively (for a detailed visualization of these structures, see Fig. S1 in the supplemental material). The blue triangle marked PK indicates the genomic region containing pseudoknot structures which was excluded from these analyses. The area corresponding to the regions encoding the nonstructural proteins (i.e., P2 and P3) is highlighted in gray. For clarity, a schematic representation of the FMDV genome is drawn to scale.

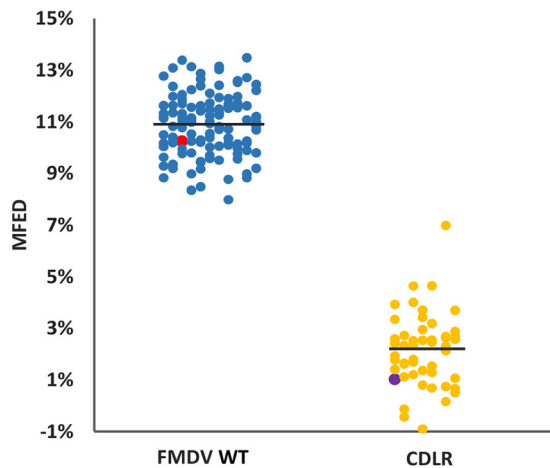


FIG 2 Comparison of average MFED values for wild-type (WT) and CDLR-scrambled sequences. Mean folding energy difference (MFED) for the regions encoding nonstructural proteins (nsps) of 118 FMDV field isolates representing all seven serotypes (blue dots), WT ptGFP replicon used in this study (red dot), and CDLR scrambled sequences (yellow dots). Among the latter is the CDLR scrambled sequence used in this study to generate replicon mutants (purple dot). To obtain CDLR-scrambled sequences, the sequence of the regions encoding the nsps of the WT replicon was permuted 50 times by codon shuffling to minimize RNA secondary structure, while preserving protein coding, native dinucleotide frequencies, and codon usage.

mean MFED value of 2.2% (SD, $\pm 1.4\%$), compared to a mean value of 10.9% (SD, $\pm 1.2\%$) for the corresponding regions of the native FMDV sequences and that of the WT FMDV replicon (Fig. 2).

To identify functional RNA structures, we divided the regions encoding the nsps of the WT replicon (ptGFP replicon) into nine consecutive fragments defined by unique restriction sites and individually permuted each fragment using the CDLR algorithm (Fig. 3A and B). To further verify the extent of changes to the RNA structure introduced by the CDLR algorithm, we used the RNAforester program implemented in the ViennaRNA Package (64, 66, 67). This compared the putative structures adopted by the CDLR-permuted regions (Fig. 3A and B) to the structures located within the corresponding regions of the WT replicon sequence. RNAforester calculates RNA secondary structure alignments based on the tree alignment model and quantifies similarity of structures in question, where the relative similarity score values equal to one represent two identical structures (64, 66, 67). With the exception of the 2C-encoding region, which exhibits some structure similarity between CDLR and WT replicon (Fig. S2), there was low structural similarity between equivalent WT and CDLR genomic fragments (Table 1). RNA structures located in the 5' and 3' UTRs were generally unaffected by any CDLR permutation of the adjacent or more distal regions encoding the nsps, with the exception of the SL1 stem-loop in the 3' UTR that was shorter by 11 pairings (Fig. S3).

CDLR replicon mutants reveal regions of secondary structure required for replication of an FMDV replicon. Next, we examined the effect of RNA structure disruption on replication of the FMDV replicon using mutant replicons containing CDLR-permuted sequences over different parts of the regions encoding the nsps. For this, we used two different continuous cell lines known to support FMDV replication: baby hamster kidney (BHK)-21 cells routinely used to grow FMDV for vaccine production and Madin-Darby bovine kidney (MDBK) cells which originate from a natural host of FMDV and appear to have functional antiviral responses (68) (Fig. 3C). The replication kinetics of the mutant replicons was compared to the WT ptGFP replicon and a replicon with an inactive polymerase (ptGFP-3D^{pol}GNN, previously described in reference 69). Since replication levels at 8 h posttransfection (hpt) were representative of the entire experiment (Fig. S4), for simplicity, data for this time point are shown. In both cell lines, all of the CDLR mutant replicons tested displayed replication kinetics

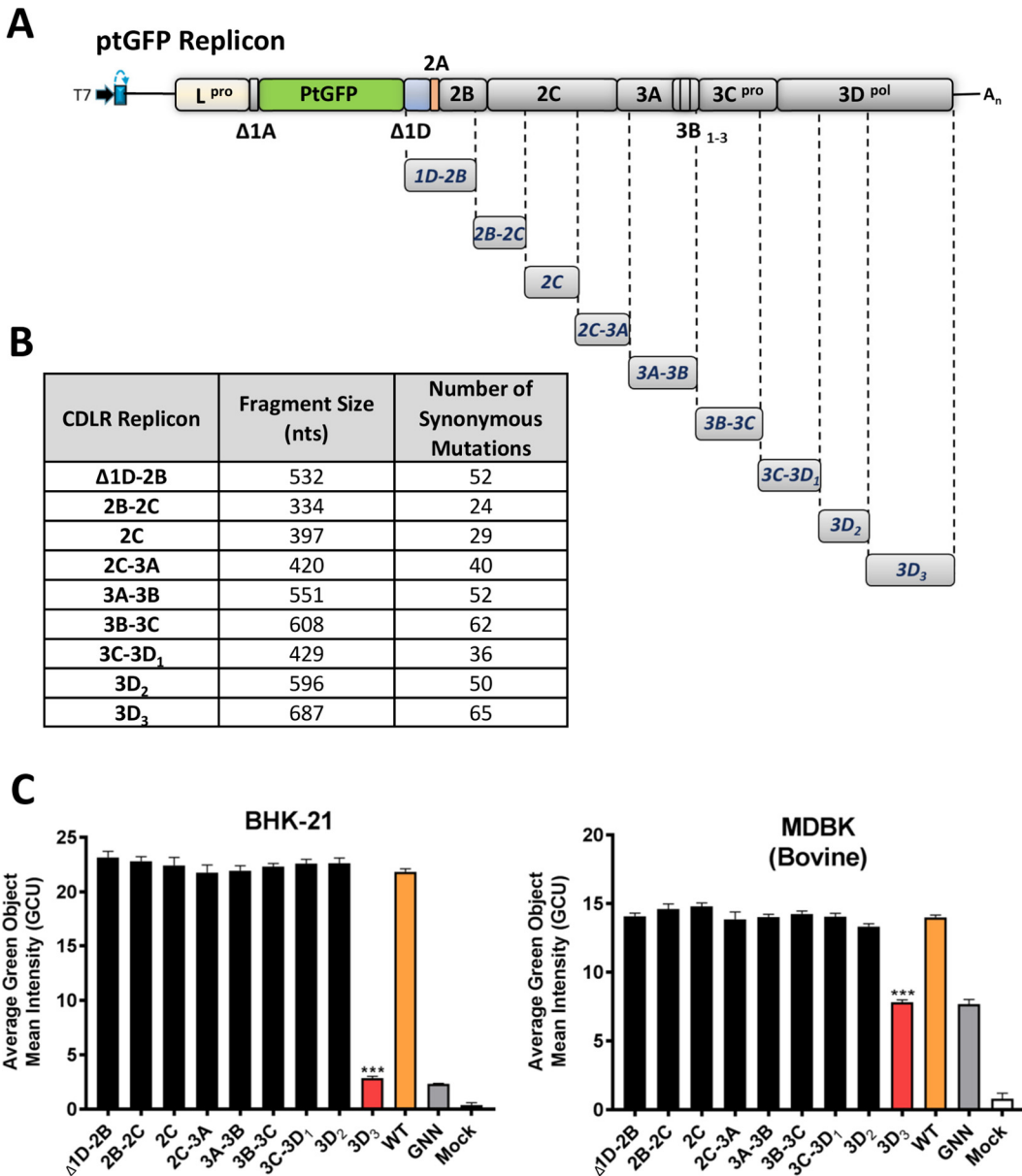


FIG 3 Replication of CDLR replicons within BHK-21 and MDBK cells. (A) Schematic representation of CDLR replicons. CDLR-permuted sequences were first inserted into a subclone encoding the nonstructural proteins (nsps) of the genome (Δ 1D-polyA) before cloning into the WT ptGFP replicon. (B) CDLR replicon insert sizes and number of mutations within each region. Regions were chosen based on unique restriction site usage within the regions encoding nsps. Mutations were introduced as described in Materials and Methods. (C) IncuCyte data represent the average cell (green object) GFP intensity (also called green calibrated unit [GCU]) per well at 8 h posttransfection. Results are the means of three independent experiments plus standard errors (error bars). Significant differences between WT ptGFP and CDLR replicons were determined (***, $P < 0.001$). The replication-incompetent 3D^{pol} active site mutant (GDD \rightarrow GNN) ptGFP-3D^{pol}GNN was used as a negative control.

comparable to the WT ptGFP replicon except for the replicon which carried a mutated sequence within the 3'-terminal part of the 3D^{pol}-encoding region (called 3D₃ here [Fig. 3C]). The replicon with mutated 3D₃-encoding region was replication defective in both cell lines, with replication levels equivalent to the negative-control replicon (ptGFP-3D^{pol}GNN; Fig. 3C). These results strongly suggest that this part of the 3D^{pol}-encoding region contains RNA structures crucial for replication of the FMDV replicon. Consistent with the inferred location of the essential RNA structures in 3D₃, CDLR permutation of the entire Δ 1D-3A- and 3A-3D₂-encoding region showed little effect on the replication kinetics (Fig. S5).

TABLE 1 Similarity comparison of RNA structures within corresponding WT and CDLR replicon genomic fragments, calculated using RNAforester program

Comparison	Relative similarity score comparing RNA structure within replicon fragments ^a												
	Δ1D-2B	2B-2C	2C	2C-3A	3A-3B	3B-3C	3C-3D ₁	3D ₂	3D ₃	S-fragment	cre ^b	IRES ^b	SL1 and SL2 ^b
WT vs CDLR	-1.33	-0.71	0.24	-0.87	-0.80	-1.69	-1.06	-0.72	-1.66	1	1	1	0.64

^aRelative similarity score comparing RNA structure located within nsps-encoding region fragments (as presented in Fig. 3A and B) of WT and CDLR replicon. A value of 1 is for two identical structures: the greater the distance from 1, the less structure similarity between two corresponding fragments. For simplicity, the output of RNAforester was rounded up to two decimal places.

^bComparison of RNA structures within the 5' and 3' UTRs of the WT and CDLR replicon acts as a control (note that while UTR regions were not permuted in this study, there was a possibility that permutation of the regions encoding the nsps might affect the pairings within UTRs).

Modification of individual stem-loops within the 3D₃ region impairs replication of an FMDV replicon. Our results indicate that the 3D₃ region of the FMDV genome contains conserved secondary RNA structures that may be necessary for replication of the FMDV replicon. Therefore, the RNA structures present in this region were investigated in more detail by visualizing each individual structure and comparing it to the corresponding scrambled region within the CDLR mutant. Analysis of corresponding sequences of FMDV field isolates (over the 3D₃ region) revealed five stem-loops (ORF-SL49 to ORF-SL53) with strong nucleotide pairing conservation, with ORF-SL52 being the most conserved structure (Fig. 4A). Variability within all structures was accommodated though the occurrence of covariant changes that preserved nucleotide pairings (Fig. 4A). Additionally, there was substantial nucleotide sequence conservation in the sequence forming the unpaired loop at the top of the stem-loop structures (i.e., in the hairpin loops) of ORF-SL49, ORF-SL50, and ORF-SL51 (Fig. 4B), implying some functional constraints on these sequences. Each of the predicted structures in the WT sequence was substantially disrupted in the CDLR scrambled mutant (Fig. 4C).

Further studies were therefore undertaken to dissect the importance of the individual stem-loops within the 3D₃ fragment for replication of the FMDV replicon. Each of the five putative RNA structures in the 3D₃ region of the WT replicon was permuted individually *in silico*, introducing the maximum number of nucleotide changes possible to disrupt the RNA structure while maintaining amino acid coding, dinucleotide frequencies, and the integrity of the neighboring RNA structures (Fig. 5 and 6A). Additionally, a replicon where all five putative RNA stem-loops were altered (ORF SL49-53^{mut}, using the same mutation strategy as for each individual stem-loop [Fig. 6A]) was designed to confirm that mutation of these particular stem-loops, and not of other elements present in the CDLR replicon with the permuted 3D₃ region, impaired RNA replication. Replication of ptGFP replicons carrying individual mutated stem-loops was tested in the same two cell lines as described above (Fig. 6). As previously observed, replication levels at 8 hpt were representative of the replication kinetics (Fig. S6). Replication of replicons with disrupted ORF-SL49 and ORF-SL50 was not affected in either cell line (Fig. 6B and Table 2). In contrast, replication of replicons with disrupted ORF-SL51 or ORF-SL52 was significantly reduced, although the effect on replication varied between the cell lines. Disruption of ORF-SL51 led to only a marginal, but statistically significant, reduction of replication in BHK-21 cells, whereas the negative effect on replication in MDBK cells was greater (Fig. 6B and Table 2). In both cell lines, disruption of ORF-SL52 reduced replication to a greater extent than disruption of ORF-SL51, with the replication profile in bovine cells being close to the replicon with an inactive polymerase (ptGFP-3D^{pol}GNN) and the replicon with the 3D₃ region mutated by the CDLR algorithm (Fig. 6B and Table 2). Replication of the replicon with disrupted ORF-SL53 was reduced only in MDBK cells (Fig. 6B and Table 2). Finally, the replicon with all five stem-loops altered (ORF SL49-53^{mut}) demonstrated replication comparable to the ptGFP-3D^{pol}GNN replication-deficient control (which gives a GFP signal due to translation of the input RNA [Fig. 6B and Table 2]).

The effect of the combined mutagenesis of stem-loops on replication of the FMDV replicon was also investigated. Initially, we tested a replicon with those four stem-loops (ORF-SL49, ORF-SL50, ORF-SL52, and ORF-SL53) mutated (ORF-SL49-50,52-53^{mut}), which

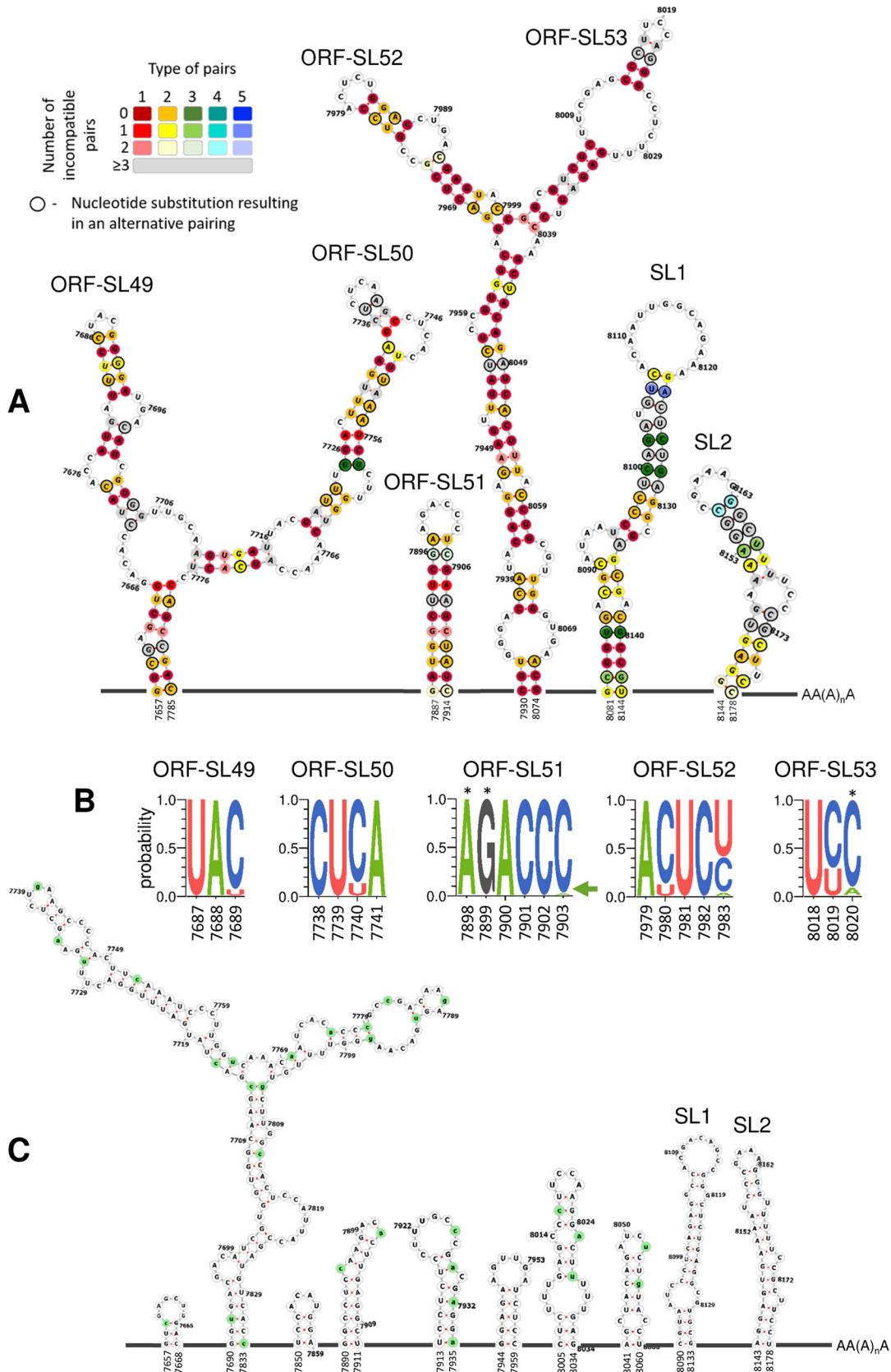


FIG 4 Schematic representation of predicted conserved RNA structures located at the 3'-terminal end of the region encoding 3D^{pol}. (A) Schematic representation of conserved (in all FMDV serotypes) RNA secondary structures located at the 3'-terminal end of the region encoding 3D^{pol} (i.e., 3D₃). Conserved putative stem-loops (ORF-SL49 to ORF-SL53) are shown, (Continued on next page)

have not been predicted before. Since mutation of ORF-SL49 and ORF-SL50 had no apparent effect on replicon replication, this replicon showed the effect of combined mutagenesis of the ORF-SL52 and ORF-SL53. While in BHK-21 cells ORF-SL49-50,52-53^{mut} replicon was attenuated at a level similar to that of the replicon containing mutation of the ORF-SL52, in the MDBK cells ORF-SL49-50,52-53^{mut} replicon showed replication levels even lower than the replicon with an inactive polymerase (Fig. 6B and Table 2), suggesting that combined mutation of the ORF-SL52 and ORF-SL53 might affect translation of the viral genome. Further constructs with two loops disrupted (ORF-SL51,52^{mut} and ORF-SL51,53^{mut}), or all three loops disrupted (ORF-SL51-53^{mut}) were tested (Fig. 7). In both cell lines, disruption of ORF-SL51 in combination with ORF-SL52 (ORF-SL51,52^{mut}), or in combination with ORF-SL52 and ORF-SL53 (ORF-SL51-53^{mut}) resulted in replication levels comparable to that of the ORF-SL49-53^{mut} negative control (Fig. 7B and Table 2). In BHK-21 cells, replication of the ORF-SL51,52^{mut} showed synergistic reduction compared to replicons with the ORF-SL51 and ORF-SL52 mutated individually (Fig. 7B and Table 2). Interestingly, disruption of ORF-SL53 in combination with ORF-SL51 (ORF-SL51,53^{mut}) resulted in a significant reduction of replicon replication in both cell lines (Table 2 and Fig. 7), although in BHK-21 cells individual mutation of ORF-SL51 and ORF-SL53 had only a marginal effect or no effect, respectively (Fig. 6). Our computational prediction of ORF-SL51,53^{mut} did not suggest any disruption of the ORF-SL52 secondary structure, which was indirectly confirmed by the experimental data where replication impairment caused by joint permutation within ORF-SL51,53^{mut} was significantly less than that of the ORF-SL51-53^{mut} (Table 2 and Fig. 7B).

Comparison of the conserved stem-loops within the FMDV 3D₃ region to structures found in the 3'-terminal 3D^{pol}-encoding region of poliovirus. Two stem-loops (referred to as loop α and β by Song et al. [38]) necessary for poliovirus (PV) replication are present in the 3'-terminus-encoding sequence of PV 3D^{pol} (37). Since PV is a member of a different genus in the family *Picornaviridae* and distantly related to FMDV, we investigated whether any of the stem-loop structures found in the 3' end of the 3D^{pol}-encoding region of the FMDV genome were similar to those present in the equivalent part of the PV genome. Therefore, we compared each of the FMDV RNA structures (ORF-SL49 to ORF-SL53) to the PV loops α and β using RNAforester. As described in Table 3, the structures identified in the 3'-terminal part of the coding region of FMDV 3D^{pol} do not appear to resemble those found in the equivalent position of the PV genome, while (using the same approach) the *cre* structures of PV and FMDV showed some structural similarity.

DISCUSSION

Many aspects of FMDV replication remain poorly understood, such as the function of RNA structures found within the ORF. Here, we revisited the RNA structural architecture of the FMDV genome and, for the first time, investigated whether the putative

FIG 4 Legend (Continued)

where two stem-loops located in the 3' UTR described before (SL1 and SL2) act as the control of the computational prediction. Nucleotide positions which form conserved pairing were color coded according to number of pairing types (red for 1 and blue for 5) and conservation of a pairing (dark shades for nucleotide pairing occurred in all FMDV isolates to light shades for lack of nucleotide pairing in two FMDV isolates). Positions colored in light gray show lack of pairing for three or more FMDV isolates. Black circular outline indicates nucleotide position where a substitution resulted in an alternative pairing (see the legend in the top left corner of panel A for detail). Unstructured regions are represented as dark gray lines and are not drawn to scale. Table S3 in the supplemental material specifies details represented graphically in the color legend in the top left corner of panel A. (B) Extent of nucleotide conservation within hairpin loops of ORF-SL49 to ORF-SL53 RNA structures. Sequence logos were generated using WebLogo 3.7.4 web server based on sequences of 118 FMDV isolates. Probability shows the extent of nucleotide occurrence at a given position. Asterisks mark positions where substitution occurs in 1 out of 118 FMDV isolates, but due to a limited resolution of the y axis, it does not appear in the sequence logos (these are A7898G, G7899A, and C8020G). The green arrow points to the C7903A substitution which due to the height of the A symbol could go unnoticed. (C) Schematic representation of RNA secondary structures located in the 3D₃ region after scrambling using the CDLR algorithm, demonstrating how RNA secondary structure in this region was changed. Mutated nucleotide positions are highlighted in green. Unstructured regions are represented as dark gray lines and are not drawn to scale. For all three panels (A to C), numbers represent nucleotide positions corresponding to the sequence of A/Brazil/1979 isolate (GenBank accession number [AY593788](https://www.ncbi.nlm.nih.gov/nuccore/AY593788)).

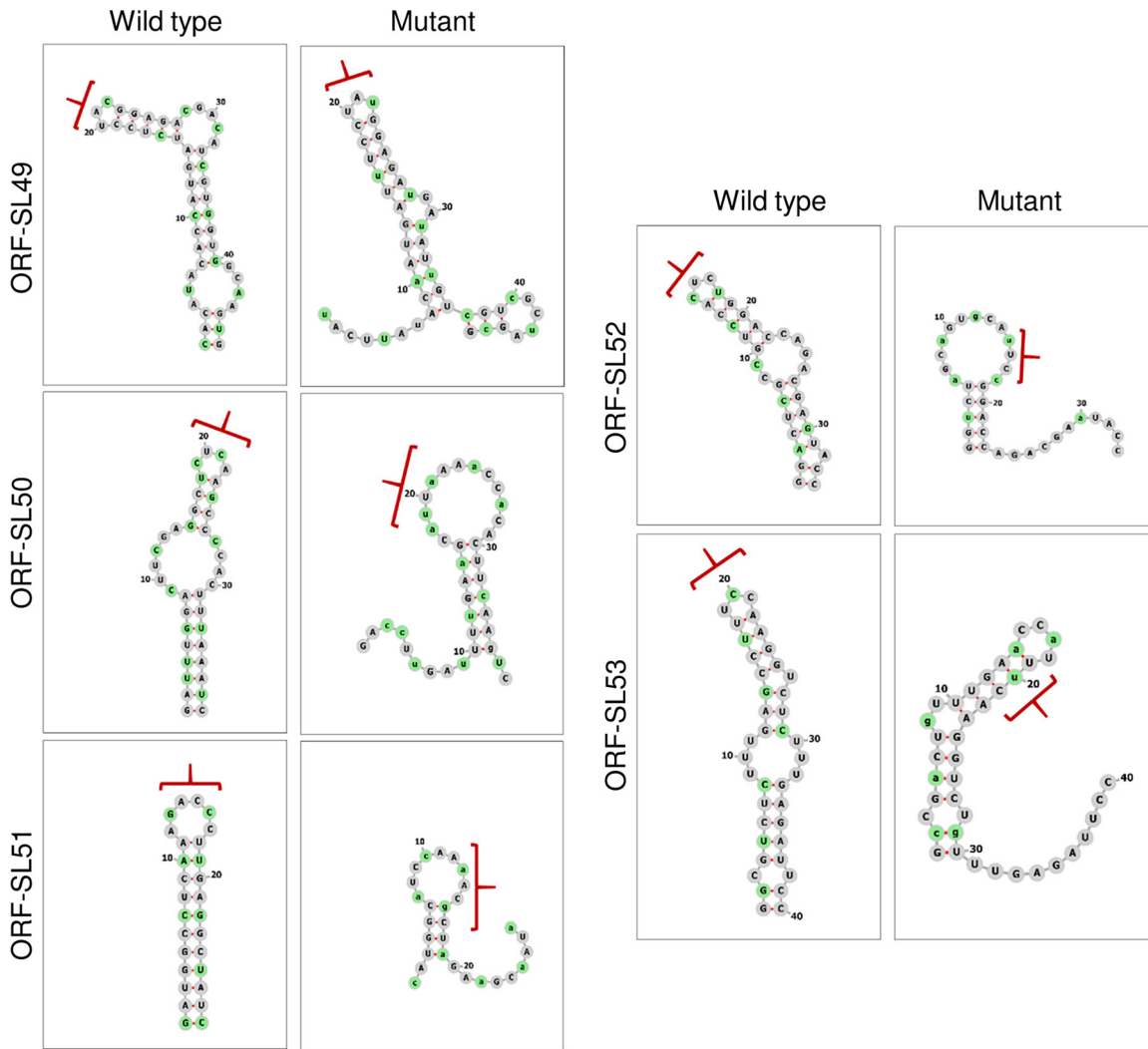


FIG 5 Disruption of the predicted RNA secondary structures by silent mutagenesis. The conserved stem-loops identified in the 3'-terminal end of the region encoding 3D^{pol} (i.e., 3D₃) of FMDV were predicted individually by Mfold for the WT ptGFP replicon. Predicted WT stem-loops were mutated to cause the highest possible disruption or change to the RNA structure without affecting neighboring stem-loops while keeping the same amino acid sequence and dinucleotide ratio (i.e., CpG and UpA). Predicted WT and mutated stem-loops visualized using the Forna web server are shown. Nucleotides highlighted in green represent mutated positions, while red brackets represent positions of the hairpin loop in the WT structures and their altered position in the disrupted structures after mutagenesis.

stem-loops localized within the ORF are required for viral genome replication. Our results are in line with previous studies showing that FMDV has extensive RNA structure throughout the genome, substantially exceeding that found in viruses of other genera of the family *Picornaviridae* (e.g., MFED value of >10% for FMDV genomic sequences compared to <4% for viral sequences belonging to genera *Enterovirus*, *Hepatovirus*, *Parechovirus*, and *Teschovirus*) (12, 56, 62). Compared to the previous structure predictions performed by Witwer et al. (12), our study identified a greater number of conserved RNA structures within the FMDV ORF (53 stem-loops, with some merging into 46 branched structures, versus 25 structures predicted previously). Since we used a larger data set than the previous authors (118 relatively diverse FMDV sequences versus 9 used by Witwer et al. [12]), it is possible that we obtained a stronger statistical signal supporting conservation of these additional structures. Importantly, we found that three of the structures within the coding region of 3D^{pol} (i.e., ORF-SL51, ORF-SL52, and ORF-SL53) were critical for efficient replication of an FMDV replicon, thereby implying that they would provide the same function during virus replication.

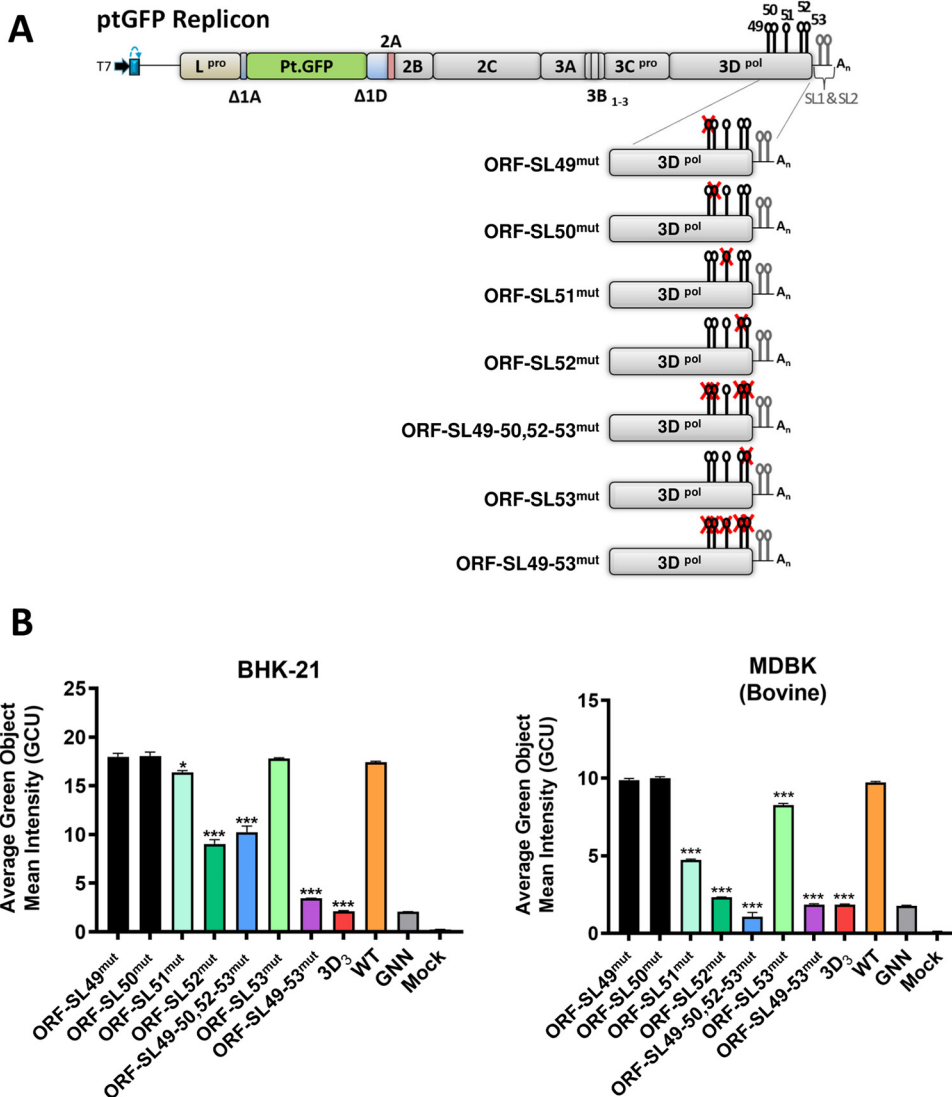


FIG 6 Effect of individual stem-loop (ORF-SL49, -50, -51, -52, and -53) mutagenesis on replication of the FMDV replicon. (A) Schematic representation of FMDV replicon constructs containing stem-loop mutations (individually, ORF-SL49^{mut}, ORF-SL50^{mut}, ORF-SL51^{mut}, ORF-SL52^{mut}, and ORF-SL53^{mut}; in combination, ORF-SL49-50,52-53^{mut}). Please see Results for detailed description of mutants. Sequence inserts containing stem-loop mutations were cloned directly into the ptGFP replicon. (B) InCuCyte data represent the average cell (green object) GFP intensity per well at 8 h posttransfection within BHK-21 and MDBK cells. Results are the means of three independent experiments plus standard errors. Significant differences between WT ptGFP and ORF-SL^{mut} replicons were determined (*, $P < 0.05$; ***, $P < 0.001$).

Despite consistently elevated MFED values, the FMDV capsid-encoding region contained only four RNA stem-loops which were conserved in all serotypes. Viral genomes characterized by high MFED values and low conservation of individual RNA structures have been observed before (70). For instance, the coding region of hepatitis C virus (HCV) showed elevated MFED values, while, except for the terminal genomic regions, the individual stem-loop structures were distinct between different HCV genotypes and even subtypes (70–72). Similarly, FMDV showed dense serotype-specific RNA structure within its capsid-encoding region, which were not shared among other serotypes (as found in reference 70 and independently here).

To identify functional RNA structures, we applied the CDLR algorithm to permute a genomic FMDV sequence (63). While the degree of possible mutagenesis is necessarily limited by protein coding, dinucleotide frequency, and codon usage constraints, the CDLR algorithm substantially disrupted secondary RNA structure of the native FMDV

TABLE 2 Summary of replication profiles of FMDV replicons after mutagenesis of conserved stem-loops localized within the 3D₃ genomic region

Cell line	Replicon profile ^a										
	ORF-SL49 ^{mut}	ORF-SL50 ^{mut}	ORF-SL51 ^{mut}	ORF-SL52 ^{mut}	ORF-SL53 ^{mut}	ORF-SL49-50, 51-52 ^{mut}	ORF-SL51,52 ^{mut}	ORF-SL51,53 ^{mut}	ORF-SL51-53 ^{mut}	ORF-SL49-53 ^{mut}	GNN ^b
BHK-21	WT	WT	94%*	52%	WT	59%	27%	60%	28%	23%	11%
MDBK	WT	WT	49%	24%	85%	11%	20%	36%	20%	20%	18%

^aSee Fig. 6 and 7 and their legends for study design and data. WT, wild-type replicon-like replication profile. Values with percentage symbols show the percentage of the WT ptGFP signal, where a significant effect on replicon replication was observed (*P* value < 0.001), except for ORF-SL51^{mut} in BHK-21 cells where *P* value = 0.02, indicated by the asterisk.

^bGNN is a replicon with an inactive polymerase. Any GFP signal is due to translation.

sequence in all regions apart from the region encoding 2C (Table 1 and Fig. S2). Since the permutation of the entire Δ1D-3A-encoding region (which resulted in more extensive changes to the RNA structure) had a minimal effect on replication of the FMDV replicon, it is safe to state that conserved RNA stem-loops within the 2C-encoding region are not essential for replication of the FMDV replicon *in vitro*.

In contrast, the CDLR scanning method identified three structures located at the 3'-terminal part of the 3D^{pol}-encoding region that were important for replication of the FMDV replicon. Of these structures, ORF-SL52 showed the highest degree of pairing conservation and appeared to be the predominant structure important for replication of the FMDV replicon. Mutation of ORF-SL51, ORF-SL52, or ORF-SL53 showed a much

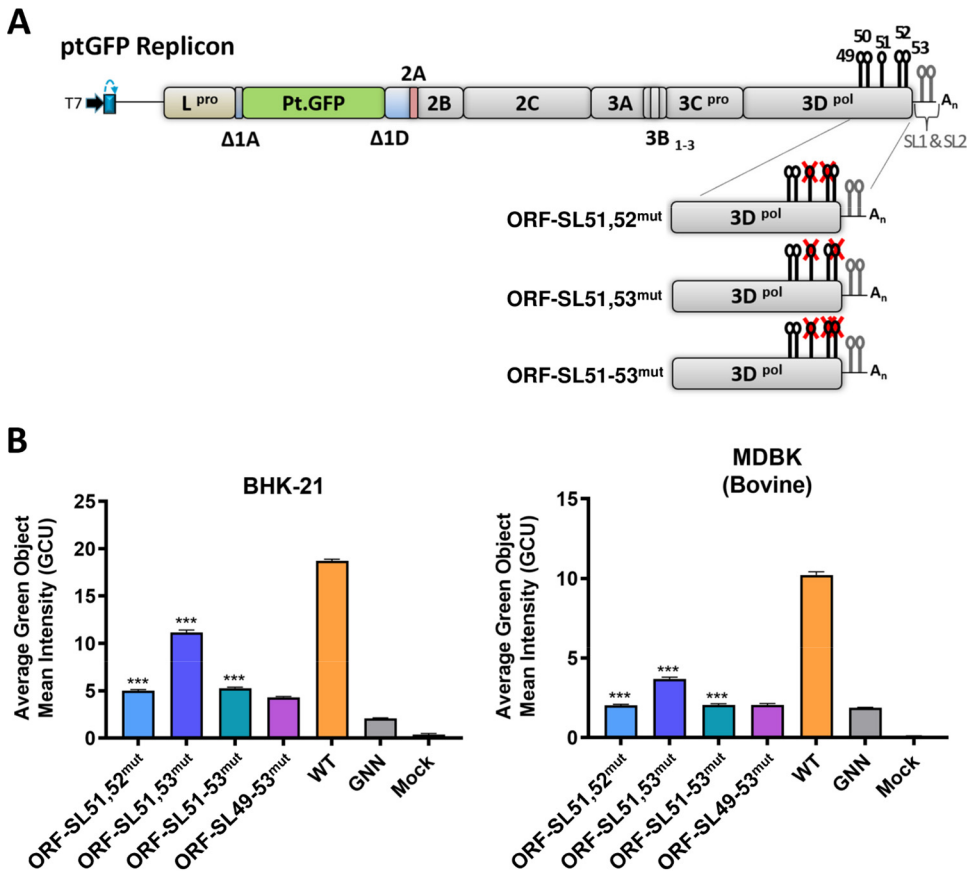


FIG 7 Effect of combined mutagenesis of stem-loops ORF-SL51, ORF-SL52, and ORF-SL53 on replication of the FMDV replicon. (A) Schematic representation of FMDV replicon constructs containing combined stem-loop mutations (ORF-SL51,52^{mut}, ORF-SL51,53^{mut}, and ORF-SL51-53^{mut}). Sequence inserts containing stem-loop mutations were cloned directly into the ptGFP replicon. (B) IncuCyte data represent the average cell (green object) GFP intensity per well at 8 h posttransfection. Results are the means of three independent experiments plus standard errors. Significant differences between WT ptGFP and ORF-SL^{mut} replicons were determined (***, *P* < 0.001).

TABLE 3 Similarity comparison of RNA structures within the 3D^{pol}-encoding region of FMDV and PV, calculated using RNAforester program

PV RNA structure	Similarity ^a of the indicated RNA structures of FMDV and PV					
	ORF-SL49	ORF-SL50	ORF-SL51	ORF-SL52	ORF-SL53	<i>cre</i> ^b
Loop α	-1.46	-1.83	-2.30	-2.10	-1.85	ND
Loop β	-1.18	-2.07	-2.52	-2.27	-2.07	ND
<i>cre</i> ^b	ND	ND	ND	ND	ND	0.30

^aA relative similarity score of 1 indicates two identical structures: the greater the distance from 1, the less structure similarity between the two compared features. For simplicity, the output of RNAforester was rounded up to two decimal places. ND, not determined.

^bComparing PV *cre* to FMDV *cre* acts as a control of the structure prediction and RNAforester analysis.

greater reduction of replicon replication in MDBK cells compared to BHK cells. MDBK cells have been shown to secrete high levels of interferon (IFN) upon stimulation (68), while BHK-21 cells are known to lack an intact IFN pathway (73, 74). Furthermore, several published results suggest that RNA structure might directly or indirectly play a role in the modulation of antiviral responses (42, 54, 75, 76). Collectively, these observations suggest that ORF-SL51, ORF-SL52, and ORF-SL53 could play additional roles in the evasion of antiviral responses, and therefore, mutation of these structures led to a drastic reduction in replication of the FMDV replicon in IFN-competent cell lines. In both cell lines tested, deletion of two or more stem-loops (ORF-SL51, ORF-SL52, and/or ORF-SL53) in combination significantly impaired replication of the replicon, suggesting that even in the absence of a fully functional antiviral pathway, all three stem-loops are important for FMDV replication. While the mechanism of stem-loop involvement in FMDV replication remains unknown, the synergistic decrease in replication of the FMDV replicon upon deletion of ORF-SL51,53 or ORF-SL52,53 in BHK-21 cells may suggest involvement of RNA-RNA interactions. Similarly to the viral genome, replication of an FMDV replicon involves viral protein synthesis, and the sequential synthesis of negative-strand (i.e., complementary) and positive-strand (i.e., genomic) viral RNA. Thus, although ORF-SL51-53 are required for replication of the replicon, further studies are required to dissect which of these processes (viral RNA translation and/or viral RNA replication) are dependent on ORF-SL51, ORF-SL52, and ORF-SL53. Interestingly, in the PV genome, stem-loops within the coding region of 3D^{pol} have been identified that are required for viral RNA synthesis (37, 38). However, these structures do not appear to share sequence or structural similarity with ORF-SL51, ORF-SL52, or ORF-SL53 in the FMDV genome.

The observation that replication of the FMDV replicon mutants with disrupted RNA structure elsewhere in the regions encoding the nsps (i.e., spanning 1D through to most of 3D^{pol}) was surprising. The maintenance of extensive conserved internal base pairing and consistently elevated MFED values observed in the relatively diverse set of FMDV isolate sequences analyzed indeed strongly argues that the RNA structures formed by those genomic regions must play some functional role in the FMDV replication cycle. It is possible that at least some of the apparently “nonfunctional” RNA structures are genome-scale ordered RNA structure (GORS) which may play a role in persistence of FMDV in its natural host (56, 62). While FMDV causes an acute disease in domestic animals (14, 77), it is known to persist in African buffalo (*Syncerus caffer*), which are a natural reservoir of the virus (78–81). Since FMDV and African buffalo are thought to have coevolved together, it is possible that GORS developed in the FMDV genome as a part of the virus-host coadaptation, where they might assist in evasion of immune recognition. The link between GORS, persistence, and ability to minimize antiviral sensing has been shown for a number of unrelated viruses (56, 62, 70, 75). Work is under way to investigate whether any of these remaining structures play a role in modulation of the antiviral sensing during FMDV replication in its natural host environment.

Although the function of the apparently nonessential RNA structures within the regions encoding the nsps remains to be defined, due to their conserved nature, they form a potential target for genome-scale attenuation of a wide range of FMDV strains.

Such a strategy could contribute to the development of live attenuated FMD vaccines that may improve on the short duration of immunity, which is a shortcoming of current inactivated vaccines. Alternatively, the manipulation of RNA structures such as ORF-SL51 to provide attenuation in bovine cells but retain efficient growth in vaccine production cell lines (BHK) could be used to enhance biosafety of inactivated vaccine production. The hazards associated with the large-scale production of killed vaccine viruses include both accidental release of virus from high containment production facilities, and the distribution and use of improperly inactivated FMD vaccines (82–84).

In summary, we have generated a comprehensive map of RNA secondary structure located within the ORF of the FMDV genome and identified novel stem-loops within the coding region for 3D^{pol} that appear critical for FMDV replication. While the function of the other conserved structures remains to be determined, they can be targeted to improve understanding of the FMDV biology. In addition, they have the potential to help develop safer FMDV vaccines, an idea which has been proposed for other viruses (6, 56, 85). We also show that usage of the CDLR algorithm can be successfully utilized to permute RNA sequences in search of functional RNA structures, which can be applied beyond viral RNA molecules using a freely available and easy to use package (63).

MATERIALS AND METHODS

Cell lines. Madin-Darby bovine kidney (MDBK) and baby hamster kidney (BHK-21) cells were obtained from the American Type Culture Collection (ATCC) and maintained in Dulbecco's modified Eagle medium (DMEM) containing either 10% fetal bovine serum (FBS) or 10% horse serum (MDBK cells) at 37°C and 5% CO₂.

FMDV sequence data set. Full genome sequences of 105 viruses were selected from GenBank database based on nucleotide distance of their 1D-encoding region, ensuring that they represent sequence variability that is known to be present between all seven FMDV serotypes (see Table S1 in the supplemental material). The 1D-encoding region is the most variable part of the FMDV genome and therefore was used to calculate distance between candidate isolates. Since sequences of SAT serotypes are the least represented on public databases, 13 additional full genome sequences of field SAT isolates (SAT 1 = 2, SAT 2 = 4, and SAT 3 = 7) were generated for the purpose of this study [isolates SAT1/TAN/3/80, SAT1/ZAM/2/88, SAT2/BOT-BUFF/7/72, SAT2/MOZ/1/70, SAT2/ZAM-BUFF/18/74, SAT2/ZIM/8/89, SAT3/BOT/209/67, SAT3/RHO/26/76, SAT3/RHO/3/75, SAT3/SAR/9/79, SAT3/ZAM/P2/96(MUL-4), SAT3/ZIM/P25/91(UR-7), and SAT3/ZIM/P26/90(HV-5)] using methodology previously described (45).

Prediction of conserved RNA structures within the FMDV genome. The genomic sequences of the 118 FMDV field isolates were aligned using the MAFFT X-INS-i algorithm which, in addition to nucleotide identity, takes into account RNA secondary structure information (86, 87). The multiple sequence alignment (MSA) was analyzed using the RNAalifold program implemented in the ViennaRNA package (64), using the following options: a ribosum scoring matrix, calculating the partition function and base pairing probability matrix in addition to the minimum free energy (MFE) structure, producing structure without lonely pairs and with dangling energies added for the bases adjacent to a helix on both sides. Then, the conserved RNA structures in the full genome were “tidied up” by removing gaps and long-distance interactions. The same was repeated for each FMDV serotype individually (using the data set described above), and serotype-specific conserved RNA structure prediction was compared to the conserved structure prediction for all 118 FMDV sequences. Stem-loops which were verified in all seven FMDV serotypes were visualized by drawing a dot plot graph using an awk script written in-house and available upon request. To visualize RNA structure located within shorter genomic fragments, a particular genomic region together with its conserved structure prediction was extracted and visualized using an on-line Forna tool implemented in the ViennaRNA Web Services (88). The extent of nucleotide conservation in sequence forming hairpin loops of RNA structures was visualized using a WebLogo 3.7.4 web server (89, 90).

Pairwise distance and MFED for full genome sequences were prepared using the Sequence Distances and Folding Energy Scan programs implemented in SSE v1.4 package (63), respectively. The MSA for MFED analysis was prepared as described above, while controls for calculation of MFED were generated by the NDR algorithm. For sequence distance analysis, the FMDV genomes were separated into three genomic regions: the 5' UTR, ORF, and 3' UTR which were aligned individually by different MAFFT algorithms. The 5' and 3' UTRs were aligned by MAFFT X-INS-i, while the nucleotide sequence of the ORF was first converted into amino acid sequence using TRANSEQ EMBOS program (91), aligned using MAFFT G-INS-i (92), and then such generated amino acid alignment was converted into nucleotide sequence using TRANALIGN EMBOS program (91). All aligned genomic fragments were manually combined into a single MSA containing FMDV whole genomes.

The average MFED values of the regions encoding the nsps of the FMDV isolates, the ptGFP replicon, and 50 CDLR-permuted ptGFP mutants were calculated as described above.

Since there appears to be a lot of ambiguity around the poly(C) tract, that region and its flanking positions were excluded from all analyses.

In silico design of mutants containing modified segments within the nonstructural-protein-encoding region. The regions encoding the nsps of the FMDV genome were chosen for mutagenesis by restriction site usage (Fig. 3A and B). To disrupt RNA secondary structures predicted in each restriction fragment of native FMDV genomes, sequences were mutated using the CDLR algorithm implemented in the Scramble Sequences Program of the SSE v1.4 package.

Structure prediction of the 3'-terminal part of the 3D^{pol}-encoding region of the WT replicon which was scrambled by the CDLR algorithm (the 3D₃ region) was generated as described above but using RNAfold (64).

To “quantify” the difference between the structures of the WT and scrambled replicons (Fig. 3A and B and Table 1), the whole genomic sequence of WT and each scrambled replicon was predicted using RNAfold, and fragments of the RNA secondary structure prediction corresponding to the permuted regions encoding the nsps (Fig. 3A and B) were compared using RNAforester and global alignment (64, 66, 67).

For each predicted RNA structure located at the 3'-terminal part of the FMDV 3D^{pol}-encoding region (ORF-SL49 to ORF-SL53), nucleotides were changed manually. Individual putative stem-loops and their mutants were predicted using RNAfold implemented in the ViennaRNA package and mfold RNA structure prediction server (93) and were visualized using Forna.

Comparison of putative RNA structures located within 3'-terminal 3D^{pol}-encoding region of FMDV and PV. Computational prediction of two conserved poliovirus (PV) RNA structures located in the 3'-terminal 3D^{pol}-encoding region (termed loop α and β as in Song et al. [38]) and described previously (37, 38) was repeated as described above. This was done as there was some discrepancy between the two publications about the exact structure of the two PV stem-loops. PV sequences representing variability of the PV 3D-encoding region (GenBank accession numbers [NC_002058.3](#), [DQ890388.1](#), [FJ769378.1](#), [EU794963.1](#), [AY560657.1](#), [HF913427.1](#), [EU794957.1](#), [EU794956.1](#), [AF538842.1](#), [EU684057.1](#), [AF405667.1](#), [AF405666.1](#), [KJ170457.1](#), [KJ170438.1](#), [KU866422.1](#), [AM884184.1](#), [AJ132961.1](#), [MG212491.1](#), [MG212488.1](#), [MG212485.1](#), [MG212463.1](#), [MG212456.1](#), [MG212441.1](#), [MG212440.1](#), [KY941933.1](#), [KY941932.1](#), [KR259355.1](#), [KC784372.1](#), [KC880377.1](#), [JX275352.1](#), [JX274995.1](#), and [KX162704.1](#)) were used. The RNA loops α and β were isolated, and their structures were aligned to the 3'-terminal part of the 3D^{pol}-encoding region containing FMDV stem-loops ORF-SL49 to ORF-SL53 using the RNAforester software and “small-in-large similarity” calculation to determine whether any of the previously described PV stem-loops were similar to any of the FMDV RNA structures identified in this study. For more detailed analysis, each isolated FMDV putative RNA stem-loop (ORF-SL49 to ORF-SL53) was directly compared to PV loop α or β using RNAforester as described above.

Clone construction. Sequences with mutations generated by the CDLR algorithm were synthesized by custom DNA synthesis (GeneArt, Life Technologies) and provided within standard cloning vectors. Since the restriction sites flanking nine CDLR regions (Fig. 3B) were not unique, final replicons containing CDLR-permuted regions were generated using subclones which allowed for usage of convenient restriction sites.

The nucleotide fragments containing mutated stem-loops ORF-SL49 to ORF-SL53 were synthesized as described above and directly cloned into the ptGFP replicon.

In vitro transcription. Replicon constructs (5 μ g) were linearized with *Ascl* (New England Biolabs) for 1 h at 37°C and purified using the E.Z.N.A. gel extraction kit (Omega Bio-Tek). Linear replicon DNA (500 ng) was added to transcription reaction mixtures at a final volume of 100 μ l containing the following: Transcription Optimized buffer (Promega), 10 mM dithiothreitol (DTT) (Promega), 100 U RNasin RNase inhibitor (Promega), 40 U T7 RNA polymerase (Promega), 20 mM ribonucleotide triphosphates (rNTPs) (Promega), and nuclease-free water. Reaction mixtures were incubated at 37°C for 2 h, and the resulting transcript integrity was assessed by agarose gel electrophoresis. RNA yield was quantified using the Quantus fluorometer (Promega), according to the manufacturer's instructions.

Cell transfection. Approximately 20 h prior to transfection, cells were seeded into 24- or 12-well plates at the appropriate cell seeding density to achieve ~80% confluence. The following day, medium was removed and replaced with FluoroBrite DMEM (Gibco) supplemented with 2% FBS and 4 mM glutamine. Replicon transcript RNA (0.5 to 1 μ g) was transfected into triplicate or quadruplicate cell monolayers using Lipofectamine 2000 transfection reagent (Thermo Fisher Scientific) per the manufacturer's recommendation.

Live cell imaging. Live cell image analysis was performed using the InCuCyte ZOOM kinetic imaging system (Essen BioScience) as described previously (65). Images were captured hourly for a period of 24 h with green fluorescent protein intensity measured using the integrated InCuCyte ZOOM image processing software. Data are shown as the average cell (green object) GFP intensity per well at 8 h posttransfection (where expression was at the maximum level).

Statistical analysis. Replicon mutants were compared to WT ptGFP using one-way analysis of variance (ANOVA). Differences between groups were considered to be significant at *P* values of <0.05. Error bars represent standard errors of the means (SEM) of multiple independent experiments. Statistical analyses were performed with GraphPad Prism 8.00 (GraphPad Software, San Diego, CA, USA).

Data availability. Full genome FMDV sequences generated as a part of this study were submitted to GenBank and are available under the following accession numbers: [MW355668](#) to [MW355680](#).

SUPPLEMENTAL MATERIAL

Supplemental material is available online only.

FIG S1, PDF file, 0.2 MB.

FIG S2, PDF file, 0.4 MB.

FIG S3, PDF file, 0.3 MB.

FIG S4, PDF file, 0.2 MB.

FIG S5, PDF file, 0.2 MB.

FIG S6, PDF file, 0.2 MB.

FIG S7, PDF file, 0.2 MB.

TABLE S1, PDF file, 0.02 MB.

TABLE S2, PDF file, 0.03 MB.

TABLE S3, PDF file, 0.04 MB.

ACKNOWLEDGMENTS

We thank colleagues in the World Reference Laboratory for Foot-and-Mouth Disease (WRLFMD) (Pirbright, United Kingdom) for providing the FMDV isolates used in this study. The Pirbright Institute receives grant-aided support from the Biotechnology and Biological Sciences Research Council (BBSRC) of the United Kingdom (projects BBS/E/I/00007035, BBS/E/I/00007036, and BBS/E/I/00007037) providing funds to cover the open access charges for this paper. This work was supported by funding from the United Kingdom Department for Environment, Food and Rural Affairs (Defra research projects SE2943 and SE2944) and BBSRC research grant BB/K003801/1.

Lidia Lasecka-Dykes, Paolo Ribeca, and Peter Simmonds performed bioinformatic analyses. Fiona Tulloch, Garry A. Luke, Lidia Lasecka-Dykes, and Sarah Gold carried out experimental work and analyzed data. Nick J. Knowles, Jemma Wadsworth, and Mehreen Azhar selected and isolated viruses. Lidia Lasecka-Dykes and Caroline F. Wright sequenced FMDV isolates and analyzed sequencing data. Fiona Tulloch, Lidia Lasecka-Dykes, Terry Jackson, Tobias J. Tuthill, Martin D. Ryan, Peter Simmonds, and Donald P. King conceived and designed the experiments. Martin D. Ryan, Terry Jackson, Tobias J. Tuthill, and Donald P. King directed the study. Martin D. Ryan, Terry Jackson, Tobias J. Tuthill, and Donald P. King acquired the funding. Lidia Lasecka-Dykes, Fiona Tulloch, and Peter Simmonds wrote the initial draft of the manuscript. All authors reviewed and edited the manuscript.

We declare that we have no conflicts of interest. The funders had no role in the design of the study, in the collection, analyses, or interpretation of data, in the writing of the manuscript, and in the decision to publish the results.

REFERENCES

- Wang J, Bakkers JM, Galama JM, Bruins Slot HJ, Pilipenko EV, Agol VI, Melchers WJ. 1999. Structural requirements of the higher order RNA kissing element in the enteroviral 3'UTR. *Nucleic Acids Res* 27:485–490. <https://doi.org/10.1093/nar/27.2.485>.
- Watts JM, Dang KK, Gorelick RJ, Leonard CW, Bess JW, Jr, Swanstrom R, Burch CL, Weeks KM. 2009. Architecture and secondary structure of an entire HIV-1 RNA genome. *Nature* 460:711–716. <https://doi.org/10.1038/nature08237>.
- Wu B, Grigull J, Ore MO, Morin S, White KA. 2013. Global organization of a positive-strand RNA virus genome. *PLoS Pathog* 9:e1003363. <https://doi.org/10.1371/journal.ppat.1003363>.
- Dethoff EA, Boerneke MA, Gokhale NS, Muhire BM, Martin DP, Sacco MT, McFadden MJ, Weinstein JB, Messer WB, Horner SM, Weeks KM. 2018. Pervasive tertiary structure in the dengue virus RNA genome. *Proc Natl Acad Sci U S A* 115:11513–11518. <https://doi.org/10.1073/pnas.1716689115>.
- Thurner C, Witwer C, Hofacker IL, Stadler PF. 2004. Conserved RNA secondary structures in Flaviviridae genomes. *J Gen Virol* 85:1113–1124. <https://doi.org/10.1099/vir.0.19462-0>.
- Firth AE. 2014. Mapping overlapping functional elements embedded within the protein-coding regions of RNA viruses. *Nucleic Acids Res* 42:12425–12439. <https://doi.org/10.1093/nar/gku981>.
- Akiyama BM, Laurence HM, Massey AR, Costantino DA, Xie XP, Yang YJ, Shi PY, Nix JC, Beckham JD, Kieft JS. 2016. Zika virus produces noncoding RNAs using a multi-pseudoknot structure that confounds a cellular exonuclease. *Science* 354:1148–1152. <https://doi.org/10.1126/science.aah3963>.
- Tuplin A, Evans DJ, Simmonds P. 2004. Detailed mapping of RNA secondary structures in core and NS5B-encoding region sequences of hepatitis C virus by RNase cleavage and novel bioinformatic prediction methods. *J Gen Virol* 85:3037–3047. <https://doi.org/10.1099/vir.0.80141-0>.
- Ferhadian D, Contrant M, Printz-Schweigert A, Smyth RP, Paillart JC, Marquet R. 2018. Structural and functional motifs in influenza virus RNAs. *Front Microbiol* 9:559. <https://doi.org/10.3389/fmicb.2018.00559>.
- Michalak P, Soszynska-Jozwiak M, Biala E, Moss WN, Keszy J, Szutkowska B, Lenartowicz E, Kierzek R, Kierzek E. 2019. Secondary structure of the segment 5 genomic RNA of influenza A virus and its application for designing antisense oligonucleotides. *Sci Rep* 9:3801. <https://doi.org/10.1038/s41598-019-40443-7>.
- Simmonds P, Karakasilioti I, Bailey D, Chaudhry Y, Evans DJ, Goodfellow IG. 2008. Bioinformatic and functional analysis of RNA secondary structure elements among different genera of human and animal caliciviruses. *Nucleic Acids Res* 36:2530–2546. <https://doi.org/10.1093/nar/gkn096>.
- Witwer C, Rauscher S, Hofacker IL, Stadler PF. 2001. Conserved RNA secondary structures in Picornaviridae genomes. *Nucleic Acids Res* 29:5079–5089. <https://doi.org/10.1093/nar/29.24.5079>.
- Tuplin A. 2015. Diverse roles and interactions of RNA structures during the replication of positive-stranded RNA viruses of humans and animals. *J Gen Virol* 96:1497–1503. <https://doi.org/10.1099/vir.0.000066>.
- Alexandersen S, Zhang Z, Donaldson AI, Garland AJ. 2003. The pathogenesis and diagnosis of foot-and-mouth disease. *J Comp Pathol* 129:1–36. [https://doi.org/10.1016/s0021-9975\(03\)00041-0](https://doi.org/10.1016/s0021-9975(03)00041-0).
- Kitching RP. 1999. Foot-and-mouth disease: current world situation. *Vaccine* 17:1772–1774. [https://doi.org/10.1016/s0264-410x\(98\)00442-3](https://doi.org/10.1016/s0264-410x(98)00442-3).
- King DP, Henstock M. 2016. OIE/FAO Foot-and-Mouth Disease Reference Laboratory Network Annual Report 2016. OIE/FAO Foot-and-Mouth Disease Reference Laboratory Network, Pirbright, United Kingdom.
- Gloster J, Sellers RF, Donaldson AI. 1982. Long-distance transport of foot-and-mouth-disease virus over the sea. *Vet Rec* 110:47–52. <https://doi.org/10.1136/vr.110.3.47>.

18. Scudamore JM, Harris DM. 2002. Control of foot and mouth disease: lessons from the experience of the outbreak in Great Britain in 2001. *Rev Sci Tech* 21:699–710. <https://doi.org/10.20506/rst.21.3.1351>.
19. Knowles NJ, Samuel AR. 2003. Molecular epidemiology of foot-and-mouth disease virus. *Virus Res* 91:65–80. [https://doi.org/10.1016/s0168-1702\(02\)00260-5](https://doi.org/10.1016/s0168-1702(02)00260-5).
20. Rweyemamu M, Roeder P, Mackay D, Sumption K, Brownlie J, Leforban Y, Valarcher JF, Knowles NJ, Saraiva V. 2008. Epidemiological patterns of foot-and-mouth disease worldwide. *Transbound Emerg Dis* 55:57–72. <https://doi.org/10.1111/j.1865-1682.2007.01013.x>.
21. Weaver GV, Domenech J, Thiermann AR, Karesh WB. 2013. Foot and mouth disease: a look from the wild side. *J Wildl Dis* 49:759–785. <https://doi.org/10.7589/2012-11-276>.
22. Di Nardo A, Knowles NJ, Paton DJ. 2011. Combining livestock trade patterns with phylogenetics to help understand the spread of foot and mouth disease in sub-Saharan Africa, the Middle East and Southeast Asia. *Rev Sci Tech* 30:63–85. <https://doi.org/10.20506/rst.30.1.2022>.
23. Samuel AR, Knowles NJ. 2001. Foot-and-mouth disease type O viruses exhibit genetically and geographically distinct evolutionary lineages (topotypes). *J Gen Virol* 82:609–621. <https://doi.org/10.1099/0022-1317-82-3-609>.
24. Kitching P, Hammond J, Jeggo M, Charleston B, Paton D, Rodriguez L, Heckert R. 2007. Global FMD control—is it an option? *Vaccine* 25:5660–5664. <https://doi.org/10.1016/j.vaccine.2006.10.052>.
25. Mason PW, Grubman MJ, Baxt B. 2003. Molecular basis of pathogenesis of FMDV. *Virus Res* 91:9–32. [https://doi.org/10.1016/s0168-1702\(02\)00257-5](https://doi.org/10.1016/s0168-1702(02)00257-5).
26. Ryan MD, Belsham GJ, King AM. 1989. Specificity of enzyme-substrate interactions in foot-and-mouth disease virus polyprotein processing. *Virology* 173:35–45. [https://doi.org/10.1016/0042-6822\(89\)90219-5](https://doi.org/10.1016/0042-6822(89)90219-5).
27. Strebel K, Beck E. 1986. A second protease of foot-and-mouth disease virus. *J Virol* 58:893–899. <https://doi.org/10.1128/JVI.58.3.893-899.1986>.
28. Vakharia VN, Devaney MA, Moore DM, Dunn JJ, Grubman MJ. 1987. Proteolytic processing of foot-and-mouth disease virus polyproteins expressed in a cell-free system from clone-derived transcripts. *J Virol* 61:3199–3207. <https://doi.org/10.1128/JVI.61.10.3199-3207.1987>.
29. Klump W, Marquardt O, Hofschneider PH. 1984. Biologically active protease of foot and mouth-disease virus is expressed from cloned viral cDNA in *Escherichia coli*. *Proc Natl Acad Sci U S A* 81:3351–3355. <https://doi.org/10.1073/pnas.81.11.3351>.
30. Belsham GJ. 2005. Translation and replication of FMDV RNA. *Curr Top Microbiol Immunol* 288:43–70. https://doi.org/10.1007/3-540-27109-0_3.
31. Donnelly MLL, Luke G, Mehrotra A, Li XJ, Hughes LE, Gani D, Ryan MD. 2001. Analysis of the aphthovirus 2A/2B polyprotein 'cleavage' mechanism indicates not a proteolytic reaction, but a novel translational effect: a putative ribosomal 'skip'. *J Gen Virol* 82:1013–1025. <https://doi.org/10.1099/0022-1317-82-5-1013>.
32. Doronina VA, Wu C, de Felipe P, Sachs MS, Ryan MD, Brown JD. 2008. Site-specific release of nascent chains from ribosomes at a sense codon. *Mol Cell Biol* 28:4227–4239. <https://doi.org/10.1128/MCB.00421-08>.
33. Ryan MD, Donnelly M, Lewis A, Mehrotra AP, Wilkie J, Gani D. 1999. A model for nonstoichiometric, cotranslational protein scission in eukaryotic ribosomes. *Bioorg Chem* 27:55–79. <https://doi.org/10.1006/bioo.1998.1119>.
34. Ryan MD, King AM, Thomas GP. 1991. Cleavage of foot-and-mouth disease virus polyprotein is mediated by residues located within a 19 amino acid sequence. *J Gen Virol* 72:2727–2732. <https://doi.org/10.1099/0022-1317-72-11-2727>.
35. Jackson RJ, Howell MT, Kaminski A. 1990. The novel mechanism of initiation of picornavirus RNA translation. *Trends Biochem Sci* 15:477–483. [https://doi.org/10.1016/0968-0004\(90\)90302-r](https://doi.org/10.1016/0968-0004(90)90302-r).
36. McKnight KL, Lemon SM. 1998. The rhinovirus type 14 genome contains an internally located RNA structure that is required for viral replication. *RNA* 4:1569–1584. <https://doi.org/10.1017/s1355838298981006>.
37. Burrill CP, Westesson O, Schulte MB, Strings VR, Segal M, Andino R. 2013. Global RNA structure analysis of poliovirus identifies a conserved RNA structure involved in viral replication and infectivity. *J Virol* 87:11670–11683. <https://doi.org/10.1128/JVI.01560-13>.
38. Song Y, Liu Y, Ward CB, Mueller S, Futcher B, Skiena S, Paul AV, Wimmer E. 2012. Identification of two functionally redundant RNA elements in the coding sequence of poliovirus using computer-generated design. *Proc Natl Acad Sci U S A* 109:14301–14307. <https://doi.org/10.1073/pnas.1211484109>.
39. Rieder E, Paul AV, Kim DW, van Boom JH, Wimmer E. 2000. Genetic and biochemical studies of poliovirus cis-acting replication element cre in relation to VPg uridylation. *J Virol* 74:10371–10380. <https://doi.org/10.1128/jvi.74.22.10371-10380.2000>.
40. Kloc A, Rai DK, Rieder E. 2018. The roles of picornavirus untranslated regions in infection and innate immunity. *Front Microbiol* 9:485. <https://doi.org/10.3389/fmicb.2018.00485>.
41. Clarke BE, Brown AL, Currey KM, Newton SE, Rowlands DJ, Carroll AR. 1987. Potential secondary and tertiary structure in the genomic RNA of foot-and-mouth disease virus. *Nucleic Acids Res* 15:7067–7079. <https://doi.org/10.1093/nar/15.17.7067>.
42. Kloc A, Diaz-San Segundo F, Schafer EA, Rai DK, Kenney M, de Los Santos T, Rieder E. 2017. Foot-and-mouth disease virus 5'-terminal S fragment is required for replication and modulation of the innate immune response in host cells. *Virology* 512:132–143. <https://doi.org/10.1016/j.virol.2017.08.036>.
43. Serrano P, Pulido MR, Saiz M, Martinez-Salas E. 2006. The 3' end of the foot-and-mouth disease virus genome establishes two distinct long-range RNA-RNA interactions with the 5' end region. *J Gen Virol* 87:3013–3022. <https://doi.org/10.1099/vir.0.82059-0>.
44. Newton SE, Carroll AR, Campbell RO, Clarke BE, Rowlands DJ. 1985. The sequence of foot-and-mouth disease virus RNA to the 5' side of the poly(C) tract. *Gene* 40:331–336. [https://doi.org/10.1016/0378-1119\(85\)90057-5](https://doi.org/10.1016/0378-1119(85)90057-5).
45. Lasecka-Dykes L, Wright CF, Di Nardo A, Logan G, Mioulet V, Jackson T, Tuthill TJ, Knowles NJ, King DP. 2018. Full genome sequencing reveals new Southern African Territories genotypes bringing us closer to understanding true variability of foot-and-mouth disease virus in Africa. *Viruses* 10:192. <https://doi.org/10.3390/v10040192>.
46. Zhu Z, Yang F, Cao W, Liu H, Zhang K, Tian H, Dang W, He J, Guo J, Liu X, Zheng H. 2019. The pseudoknot region of the 5' untranslated region is a determinant of viral tropism and virulence of foot-and-mouth disease virus. *J Virol* 93:e02039-18. <https://doi.org/10.1128/JVI.02039-18>.
47. Lopez de Quinto S, Martinez-Salas E. 1997. Conserved structural motifs located in distal loops of aphthovirus internal ribosome entry site domain 3 are required for internal initiation of translation. *J Virol* 71:4171–4175. <https://doi.org/10.1128/jvi.71.5.4171-4175.1997>.
48. Belsham GJ, Brangwyn JK. 1990. A region of the 5' noncoding region of foot-and-mouth disease virus RNA directs efficient internal initiation of protein synthesis within cells: involvement with the role of L protease in translational control. *J Virol* 64:5389–5395. <https://doi.org/10.1128/JVI.64.11.5389-5395.1990>.
49. Kuhn R, Luz N, Beck E. 1990. Functional analysis of the internal translation initiation site of foot-and-mouth disease virus. *J Virol* 64:4625–4631. <https://doi.org/10.1128/JVI.64.10.4625-4631.1990>.
50. Serrano P, Ramajo J, Martinez-Salas E. 2009. Rescue of internal initiation of translation by RNA complementation provides evidence for a distribution of functions between individual IRES domains. *Virology* 388:221–229. <https://doi.org/10.1016/j.virol.2009.03.021>.
51. Mason PW, Bezborodova SV, Henry TM. 2002. Identification and characterization of a cis-acting replication element (cre) adjacent to the internal ribosome entry site of foot-and-mouth disease virus. *J Virol* 76:9686–9694. <https://doi.org/10.1128/jvi.76.19.9686-9694.2002>.
52. Nayak A, Goodfellow IG, Belsham GJ. 2005. Factors required for the uridylation of the foot-and-mouth disease virus 3B1, 3B2, and 3B3 peptides by the RNA-dependent RNA polymerase (3D^{pol}) in vitro. *J Virol* 79:7698–7706. <https://doi.org/10.1128/JVI.79.12.7698-7706.2005>.
53. Saiz M, Gomez S, Martinez-Salas E, Sobrino F. 2001. Deletion or substitution of the aphthovirus 3' NCR abrogates infectivity and virus replication. *J Gen Virol* 82:93–101. <https://doi.org/10.1099/0022-1317-82-1-93>.
54. Pulido MR, Sobrino F, Borrego B, Saiz M. 2009. Attenuated foot-and-mouth disease virus RNA carrying a deletion in the 3' noncoding region can elicit immunity in swine. *J Virol* 83:3475–3485. <https://doi.org/10.1128/JVI.01836-08>.
55. Logan G, Newman J, Wright CF, Lasecka-Dykes L, Haydon DT, Cottam EM, Tuthill TJ. 2018. Deep sequencing of foot-and-mouth disease virus reveals RNA sequences involved in genome packaging. *J Virol* 92:e01159-17. <https://doi.org/10.1128/JVI.01159-17>.
56. Simmonds P, Tuplin A, Evans DJ. 2004. Detection of genome-scale ordered RNA structure (GORS) in genomes of positive-stranded RNA viruses: implications for virus evolution and host persistence. *RNA* 10:1337–1351. <https://doi.org/10.1261/rna.7640104>.
57. Seffens W, Digby D. 1999. mRNAs have greater negative folding free energies than shuffled or codon choice randomized sequences. *Nucleic Acids Res* 27:1578–1584. <https://doi.org/10.1093/nar/27.7.1578>.
58. Bonnet E, Wuys J, Rouze P, Van de Peer Y. 2004. Evidence that microRNA precursors, unlike other non-coding RNAs, have lower folding free

- energies than random sequences. *Bioinformatics* 20:2911–2917. <https://doi.org/10.1093/bioinformatics/bth374>.
59. Zuker M. 1989. On finding all suboptimal foldings of an RNA molecule. *Science* 244:48–52. <https://doi.org/10.1126/science.2468181>.
 60. Rivas E, Eddy SR. 2000. Secondary structure alone is generally not statistically significant for the detection of noncoding RNAs. *Bioinformatics* 16:583–605. <https://doi.org/10.1093/bioinformatics/16.7.583>.
 61. Workman C, Krogh A. 1999. No evidence that mRNAs have lower folding free energies than random sequences with the same dinucleotide distribution. *Nucleic Acids Res* 27:4816–4822. <https://doi.org/10.1093/nar/27.24.4816>.
 62. Davis M, Sagan SM, Pezacki JP, Evans DJ, Simmonds P. 2008. Bioinformatic and physical characterizations of genome-scale ordered RNA structure in mammalian RNA viruses. *J Virol* 82:11824–11836. <https://doi.org/10.1128/JVI.01078-08>.
 63. Simmonds P. 2012. SSE: a nucleotide and amino acid sequence analysis platform. *BMC Res Notes* 5:50. <https://doi.org/10.1186/1756-0500-5-50>.
 64. Lorenz R, Bernhart SH, Honer Zu Siederdisen C, Tafer H, Flamm C, Stadler PF, Hofacker IL. 2011. ViennaRNA package 2.0. *Algorithms Mol Biol* 6:26. <https://doi.org/10.1186/1748-7188-6-26>.
 65. Tulloch F, Pathania U, Luke GA, Nicholson J, Stonehouse NJ, Rowlands DJ, Jackson T, Tuthill T, Haas J, Lamond AI, Ryan MD. 2014. FMDV replicons encoding green fluorescent protein are replication competent. *J Virol Methods* 209:35–40. <https://doi.org/10.1016/j.jviromet.2014.08.020>.
 66. Hoechsmann M, Toeller T, Giegerich R, Kurtz S. 2003. Local similarity of RNA secondary structures, p 159–168. *In Proceedings of the 2003 IEEE Bioinformatics Conference*. CSB2003. Institute of Electrical and Electronics Engineers, New York, NY.
 67. Jiang T, Wang LS, Zhang KZ. 1995. Alignment of trees - an alternative to Tree Edit. *Theor Comput Sci* 143:137–148. [https://doi.org/10.1016/0304-3975\(95\)80029-9](https://doi.org/10.1016/0304-3975(95)80029-9).
 68. Luna VER, Luk ADH, Tying SK, Hellman JM, Lefkowitz SS. 1984. Properties of bovine interferons. *Experientia* 40:1410–1412. <https://doi.org/10.1007/BF01951916>.
 69. Herod MR, Lourdas EA, Ward JC, Tulloch F, Rowlands DJ, Stonehouse NJ. 2015. Employing transposon mutagenesis to investigate foot-and-mouth disease virus replication. *J Gen Virol* 96:3507–3518. <https://doi.org/10.1099/jgv.0.000306>.
 70. Simmonds P, Cuyppers L, Irving WL, McLauchlan J, Cooke GS, Barnes E, STOP-HCV Consortium, Ansari MA. 2020. Impact of virus subtype and host IFNL4 genotype on large-scale RNA structure formation in the genome of hepatitis C virus. *RNA* 26:1541–1556. <https://doi.org/10.1261/rna.075465.120>.
 71. Pirakitikulr N, Kohlway A, Lindenbach BD, Pyle AM. 2016. The coding region of the HCV genome contains a network of regulatory RNA structures. *Mol Cell* 62:111–120. <https://doi.org/10.1016/j.molcel.2016.01.024>.
 72. Mauger DM, Golden M, Yamane D, Williford S, Lemon SM, Martin DP, Weeks KM. 2015. Functionally conserved architecture of hepatitis C virus RNA genomes. *Proc Natl Acad Sci U S A* 112:3692–3697. <https://doi.org/10.1073/pnas.1416266112>.
 73. Conzelmann KK. 2004. Reverse genetics of Mononegavirales. *Curr Top Microbiol Immunol* 283:1–41. https://doi.org/10.1007/978-3-662-06099-5_1.
 74. Schlender J, Bossert B, Buchholz U, Conzelmann KK. 2000. Bovine respiratory syncytial virus nonstructural proteins NS1 and NS2 cooperatively antagonize alpha/beta interferon-induced antiviral response. *J Virol* 74:8234–8242. <https://doi.org/10.1128/jvi.74.18.8234-8242.2000>.
 75. Witteveldt J, Blundell R, Maarleveld JJ, McFadden N, Evans DJ, Simmonds P. 2014. The influence of viral RNA secondary structure on interactions with innate host cell defences. *Nucleic Acids Res* 42:3314–3329. <https://doi.org/10.1093/nar/gkt1291>.
 76. Smyth RP, Negroni M, Lever AM, Mak J, Kenyon JC. 2018. RNA structure—a neglected puppet master for the evolution of virus and host immunity. *Front Immunol* 9:2097. <https://doi.org/10.3389/fimmu.2018.02097>.
 77. Zhang ZD, Alexandersen S. 2004. Quantitative analysis of foot-and-mouth disease virus RNA loads in bovine tissues: implications for the site of viral persistence. *J Gen Virol* 85:2567–2575. <https://doi.org/10.1099/vir.0.80011-0>.
 78. Condy JB, Hedger RS, Hamblin C, Barnett IT. 1985. The duration of the foot-and-mouth disease virus carrier state in African buffalo (i) in the individual animal and (ii) in a free-living herd. *Comp Immunol Microbiol Infect Dis* 8:259–265. [https://doi.org/10.1016/0147-9571\(85\)90004-9](https://doi.org/10.1016/0147-9571(85)90004-9).
 79. Vosloo W, Dwarka RM, Bastos ADS, Esterhuysen JJ, Sahle M, Sangare O. 2004. Molecular epidemiological studies of foot-and-mouth disease virus in sub-Saharan Africa indicate the presence of large numbers of topotypes: implications for local and international control. Session of the Research Group of the Standing Technical Committee of the European Commission for the Control of Foot-and-Mouth Disease (EUFMD) at Crete, Greece.
 80. Vosloo W, de Klerk LM, Boshoff CI, Botha B, Dwarka RM, Keet D, Haydon DT. 2007. Characterisation of a SAT-1 outbreak of foot-and-mouth disease in captive African buffalo (*Syncerus caffer*): clinical symptoms, genetic characterisation and phylogenetic comparison of outbreak isolates. *Vet Microbiol* 120:226–240. <https://doi.org/10.1016/j.vetmic.2006.11.002>.
 81. Thomson GR, Vosloo W, Esterhuysen JJ, Bengis RG. 1992. Maintenance of foot and mouth disease viruses in buffalo (*Syncerus caffer* Sparrman, 1779) in southern Africa. *Rev Sci Tech* 11:1097–1107. <https://doi.org/10.20506/rst.11.4.646>.
 82. Independent Review Group. 2007. Independent review of the safety of UK facilities handling foot-and-mouth disease virus. Chaired by Prof. Brian G. Spratt. Independent Review Group, Department for Environment, Food and Rural Affairs (Defra), London, United Kingdom.
 83. Department for Environment, Food and Rural Affairs. 2007. A review of the regulatory framework for handling animal pathogens. Chaired by Sir Bill Callaghan. Department for Environment, Food and Rural Affairs (Defra), London, United Kingdom.
 84. Sangula AK, Siegismund HR, Belsham GJ, Balinda SN, Masembe C, Muwanika VB. 2011. Low diversity of foot-and-mouth disease serotype C virus in Kenya: evidence for probable vaccine strain re-introductions in the field. *Epidemiol Infect* 139:189–196. <https://doi.org/10.1017/S0950268810000580>.
 85. Runckel C, Westesson O, Andino R, DeRisi JL. 2013. Identification and manipulation of the molecular determinants influencing poliovirus recombination. *PLoS Pathog* 9:e1003164. <https://doi.org/10.1371/journal.ppat.1003164>.
 86. Katoh K, Toh H. 2008. Improved accuracy of multiple ncRNA alignment by incorporating structural information into a MAFFT-based framework. *BMC Bioinformatics* 9:212. <https://doi.org/10.1186/1471-2105-9-212>.
 87. Katoh K, Asimenos G, Toh H. 2009. Multiple alignment of DNA sequences with MAFFT. *Methods Mol Biol* 537:39–64. https://doi.org/10.1007/978-1-59745-251-9_3.
 88. Kerpedjiev P, Hammer S, Hofacker IL. 2015. Forna (force-directed RNA): simple and effective online RNA secondary structure diagrams. *Bioinformatics* 31:3377–3379. <https://doi.org/10.1093/bioinformatics/btv372>.
 89. Schneider TD, Stephens RM. 1990. Sequence logos: a new way to display consensus sequences. *Nucleic Acids Res* 18:6097–6100. <https://doi.org/10.1093/nar/18.20.6097>.
 90. Crooks GE, Hon G, Chandonia JM, Brenner SE. 2004. WebLogo: a sequence logo generator. *Genome Res* 14:1188–1190. <https://doi.org/10.1101/gr.849004>.
 91. Madeira F, Park YM, Lee J, Buso N, Gur T, Madhusoodanan N, Basutkar P, Tivey ARN, Potter SC, Finn RD, Lopez R. 2019. The EMBL-EBI search and sequence analysis tools APIs in 2019. *Nucleic Acids Res* 47:W636–W641. <https://doi.org/10.1093/nar/gkz268>.
 92. Katoh K, Kuma K, Toh H, Miyata T. 2005. MAFFT version 5: improvement in accuracy of multiple sequence alignment. *Nucleic Acids Res* 33:511–518. <https://doi.org/10.1093/nar/gki198>.
 93. Zuker M. 2003. Mfold web server for nucleic acid folding and hybridization prediction. *Nucleic Acids Res* 31:3406–3415. <https://doi.org/10.1093/nar/gkg595>.